JCI insight

Reciprocal regulation of Th2 and Th17 cells by PAD2-mediated citrullination

Bo Sun, … , Paul R. Thompson, I-Cheng Ho

JCI Insight. 2019;4(22):e129687. https://doi.org/10.1172/jci.insight.129687.

Research Article Immunology

Graphical abstract

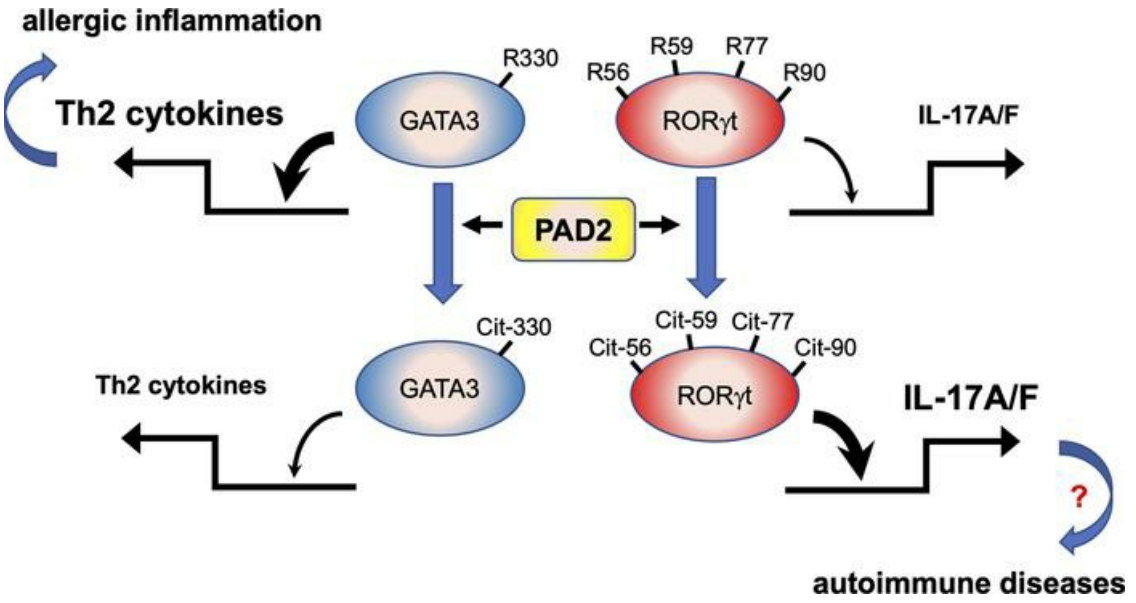

JCI insight

RESEARCH ARTICLE

Reciprocal regulation of Th2 and Th17 cells by PAD2-mediated citrullination

Bo Sun,[1,2] Hui-Hsin Chang,[1,2] Ari Salinger,[3] Beverly Tomita,[1,2] Mandar Bawadekar,[4] Caitlyn L. Holmes,[4,5] Miriam A. Shelef,[4,6] Eranthie Weerapana,[7] Paul R. Thompson,[3] and I-Cheng Ho[1,2]

[1]Division of Rheumatology, Inflammation, and Immunity, Department of Medicine, Brigham and Women's Hospital, Boston, Massachusetts, USA. [2]Harvard Medical School, Boston, Massachusetts, USA. [3]Department of Biochemistry and Molecular Pharmacology, University of Massachusetts Medical School, Worcester, Massachusetts, USA. [4]Department of Medicine and [5]Department of Pathology and Laboratory Medicine, University of Wisconsin-Madison, Madison, Wisconsin, USA. [6]William S. Middleton Memorial Veterans Hospital, Madison, Wisconsin, USA. [7]Department of Chemistry, Boston College, Chestnut Hill, Massachusetts, USA.

Dysregulated citrullination, a unique form of posttranslational modification catalyzed by the peptidylarginine deiminases (PADs), has been observed in several human diseases, including rheumatoid arthritis. However, the physiological roles of PADs in the immune system are still poorly understood. Here, we report that global inhibition of citrullination enhances the differentiation of type 2 helper T (Th2) cells but attenuates the differentiation of Th17 cells, thereby increasing the susceptibility to allergic airway inflammation. This effect on Th cells is due to inhibition of PAD2 but not PAD4. Mechanistically, PAD2 directly citrullinates GATA3 and RORγt, 2 key transcription factors determining the fate of differentiating Th cells. Citrullination of R330 of GATA3 weakens its DNA binding ability, whereas citrullination of 4 arginine residues of RORγt strengthens its DNA binding. Finally, PAD2-deficient mice also display altered Th2/Th17 immune response and heightened sensitivity to allergic airway inflammation. Thus, our data highlight the potential and caveat of PAD2 as a therapeutic target of Th cell–mediated diseases.

Introduction

The function of many proteins is heavily influenced by their posttranslational modifications. One unique form of such modifications is citrullination, also called deimination, in which peptidylarginine is irreversibly converted to the noncoding amino acid peptidylcitrulline. This process is catalyzed by the peptidylarginine deiminases, including PAD1–4 and PAD6 (1). Each PAD has a different pattern of tissue distribution. For example, hematopoietic cells express mainly PAD2 and PAD4, with neutrophils expressing the highest level of PAD4. PAD6 is expressed almost exclusively in oocytes, whereas PAD1 and PAD3 are expressed mainly in nonhematopoietic cells. Given their pattern of tissue distribution, it is believed that PADs have both unique and overlapping substrates.

By converting positively charged peptidylarginine to neutral peptidylcitrulline, citrullination has the potential of altering protein folding, interaction, degradation, and function. For example, PAD1 and PAD6 are indispensable for early embryogenesis (2, 3), whereas PAD4-mediated citrullination of histones is essential for the formation of neutrophil extracellular traps in some experimental settings (4). However, aberrant citrullination very likely contributes to the pathogenesis of several human diseases. For example, rheumatoid arthritis (RA) is characterized by the presence of anti-citrullinated protein antibodies (5, 6). Several major risk factors of RA, such as periodontitis, smoking, the rs2476601 SNP of PTPN22, and family history, are associated with local or systemic hypercitrullination (7–10). In addition, inhibition of PADs is beneficial in several animal models of human diseases, including inflammatory arthritis, lupus, colitis, and cancer (1). Despite these observations, the regulatory roles of PADs and citrullination in adaptive immune cells and other human diseases, such as allergic inflammation, are still poorly understood.

$CD4^+$ Th cells play a key role in the immune defense against invading pathogens but can also cause autoimmune and allergic diseases if their functions are not regulated properly (11). Several functional subsets of effector Th cells, including Th1, Th2, and Th17 cells, have been discovered. The differentiation of these subsets is critically regulated by several subset-specific transcription factors, such as T-bet for Th1

Authorship note: BS and HHC contributed equally.

Conflict of interest: The authors have declared that no conflict of interest exists.

Submitted: April 19, 2019
Accepted: October 16, 2019
Published: November 14, 2019.

Reference information: *JCI Insight*. 2019;4(22):e129687. https://doi.org/10.1172/jci.insight.129687.

cells, GATA3 for Th2 cells, and RORγt for Th17 cells. While the activity of these transcription factors usually correlates with their protein levels, which are regulated mainly by transcription, their activity is also subject to regulation by several posttranslational modifications. For example, phosphorylation by p38 and methylation of Arg261 enhance the function of GATA3 (12, 13); the activity of RORγt can be influenced by its acetylation (14, 15). We recently discovered that overexpression of PAD2 in PBMC of healthy donors suppressed anti-CD3–induced expression of Th2 cytokines but had an opposite effect on the expression of Th17 cytokines (10). This observation suggests that the differentiation/function of Th cells can be modulated by citrullination. However, it is unknown whether PAD2 at a physiological level can still regulate the differentiation of Th cells and, if it does, what its mechanism of action is.

Here, we demonstrate that global inhibition of citrullination alters the differentiation of Th cells and augments allergic airway inflammation. This effect is recapitulated by inhibition of PAD2 but not PAD4. We further show that PAD2-mediated citrullination of GATA3 and RORγt modulates their DNA binding activity, thereby reciprocally regulating the differentiation of Th2 and Th17 cells in vitro and in vivo. Taken together, our data depict a potentially novel mechanism by which citrullination fine-tunes the Th immune response and modulates allergic airway inflammation.

Results

Modulation of in vitro and in vivo differentiation of Th cells by global inhibition of citrullination. We first used anti–citrullinated histone H3 (cit-H3), which has been validated in PAD4-KO neutrophils (4), to compare the status of citrullination among naive and various effector Th cells. We found a trend of higher levels of cit-H3 in effector Th cells compared with naive Th cells, but we found no significant difference among the effector subsets (Figure 1A). Restimulation of the effector Th cells with anti-CD3 also did not significantly alter the level of cit-H3.

We subsequently differentiated and restimulated mouse Th cells in the presence of Cl-amidine (Cl-am), a pan-PAD inhibitor. Cl-am dose-dependently reduced the level of cit-H3 but did not completely inhibit the citrullination of H3, even at a concentration (100 μM) that was tolerable to Th cells (Figure 1B). It also subtly inhibited the proliferation of differentiating Th cells (Supplemental Figure 1, A and B; supplemental material available online with this article; https://doi.org/10.1172/jci.insight.129687DS1). Interestingly, Cl-am dose-dependently increased the expression of IL-4, IL-5, and IL-13 by Th2 cells but reduced the expression of IL-17A and IL-17F by Th17 cells (Figure 1C). By contrast, Cl-am had little impact on the expression of IFN-γ by Th1 cells. Cl-am also attenuated the differentiation of primary human Th17 cells and modestly enhanced the differentiation of human Th2 cells from 4 of 5 healthy donors (Figure 1D).

Excessive Th2 immune response is pathogenic in allergic airway inflammation. To further characterize the effect of global citrullination on Th2 immune response in vivo, we i.p. immunized WT C57BL/6 mice with ovalbumin in aluminum hydroxide (alum), followed by challenges with aerosolized ovalbumin to induce allergic airway inflammation. The mice were treated with either DMSO or Cl-am. In agreement with the data shown in Figure 1C, splenocytes from Cl-am–treated mice produced more IL-4 but less IL-17A in response to in vitro challenge with ovalbumin (Figure 1E). There was also a trend of higher level of ovalbumin-specific IgE but lower level of ovalbumin-specific IgG1 in the serum of Cl-am–treated mice (Figure 1F), reflecting the impact of heightened Th2 response on the B cell compartment. No such trend was observed for the levels of total IgE and IgG1 in serum (Supplemental Figure 1C). Furthermore, Cl-am treatment enhanced airway inflammation (Figure 1G), resulting in an increase in total cell number and percentage of eosinophils in lavage (Figure 1, H and I).

Inhibition of PAD2 but not PAD4 phenocopies the effects of Cl-am. To determine inhibition of which PAD is responsible for the effect of Cl-am, we first examined the expression of various PADs in Th cells. Transcript level of PAD2, albeit low, was the highest among all PADs in naive Th cells (Figure 2A). By contrast, primary macrophages expressed more PAD4 than PAD2. The level of PAD2 transcripts was higher in effector Th cells. This trend was also observed in the level of PAD2 proteins (Figure 2B). The induction of PAD2 was readily observed 2 days after activation, regardless of polarizing conditions (Figure 2C). Anti-CD3, but not anti-CD28 or IL-2, alone was sufficient to induce the expression of PAD2 (Figure 2D). This induction by anti-CD3 was blocked by cyclosporine A or sotrastaurin (Figure 2E), indicating that both calcium and PKC signaling pathways are essential for the induction of PAD2. We subsequently treated differentiating Th cells with a PAD2-specific inhibitor AFM30a (16) and found that AFM30a phenocopied the effect of Cl-am (Figure 2F). The expression of PAD4 in Th cells has been

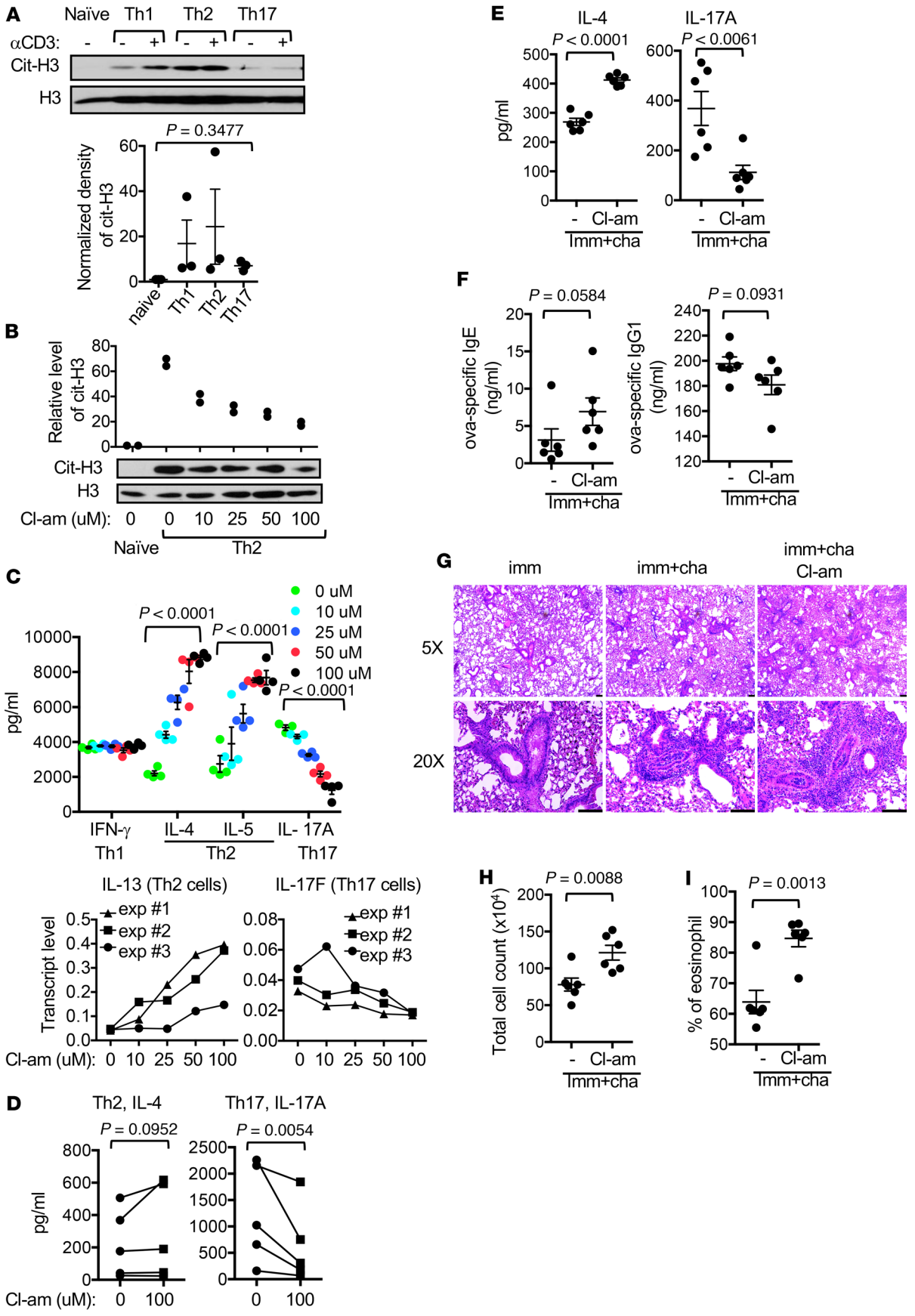
A
Naïve
Th1
Th2
Th17
αCD3:
Cit-H3
H3
P = 0.3477
Normalized density of cit-H3
naive
Th1
Th2
Th17
B
Relative level of cit-H3
Cit-H3
H3
Cl-am (uM): 0 0 10 25 50 100
Naïve
Th2
C
P < 0.0001
P < 0.0001
P < 0.0001
0 uM
10 uM
25 uM
50 uM
100 uM
pg/ml
IFN-γ
IL-4
IL-5
IL- 17A
Th1
Th2
Th17
IL-13 (Th2 cells)
IL-17F (Th17 cells)
exp #1
exp #2
exp #3
Transcript level
Cl-am (uM): 0 10 25 50 100
D
Th2, IL-4
Th17, IL-17A
P = 0.0952
P = 0.0054
pg/ml
Cl-am (uM): 0 100
E
IL-4
IL-17A
P < 0.0001
P < 0.0061
pg/ml
- Cl-am
Imm+cha
F
P = 0.0584
P = 0.0931
ova-specific IgE (ng/ml)
ova-specific IgG1 (ng/ml)
- Cl-am
Imm+cha
G
imm
imm+cha
imm+cha Cl-am
5X
20X
H
P = 0.0088
Total cell count (x10⁴)
- Cl-am
Imm+cha
I
P = 0.0013
% of eosinophil
- Cl-am
Imm+cha

Figure 1. Modulation of in vivo and in vitro differentiation of Th cells by global inhibition of citrullination. (**A**) Indicated C57BL/6 Th cells were left unstimulated (–) or restimulated with anti-CD3 (+) overnight. The level of cit-H3 was examined with Western blotting using anti–cit-H3. The normalized density of cit-H3 is shown in the bar graph (n = 3, 1-way ANOVA). (**B** and **C**) C57BL/6 effector Th cells were generated in the presence of Cl-am at indicated concentrations for 5 days. Whole Th2 extract was examined with Western blotting using indicated antibodies. Representative blots and normalized density of cit-H3 from 2 experiments are shown in **B**. The expression of indicated cytokines by the Th cells after restimulation with anti-CD3 is shown in **C** (n = 4, 1-way ANOVA)**.** (**D**) Primary human Th cells from 5 healthy donors were differentiated in vitro into Th2 or Th17 cells in the presence or absence of Cl-am (100 μM). The production of IL-4 and IL-17A after restimulation with anti-CD3 was quantified with ELISA. Data points from the same donors are connected with lines (1-tailed paired Student's t test). (**E**–**I**) Allergic airway inflammation was induced in C57BL/6 mice (n = 6 per group) in the absence or presence of Cl-am. Splenocytes were restimulated with ovalbumin for 72 hours. The levels of IL-4 and IL-17A in supernatant are shown in **E**. Imm, immunized; cha, challeneged. The levels of ovalbumin-specific (ova-specific) IgE and IgG1 in serum are shown in **F**. Representative H&E staining of the lung tissue is shown in **G**. Scale bars: 100 μm. The total number of cells (**H**) and the percentage of eosinophils (**I**) in bronchial lavage are also shown. Statistical analysis for **E**, **F**, **H**, and **I** was performed with 2-tailed Student's t test.

reported. However, PAD4-specific inhibitor GSK199 (17) had no impact on the differentiation of Th2 or Th17 cells. Neither inhibitor affected the differentiation of Th1 cells.

To confirm that the effect of Cl-am or AFM30a was indeed due to inhibition of PAD2 but not off-target effects, we further examined the differentiation of PAD2-KO Th cells. Deficiency of PAD2 had little impact on the proliferation and activation of Th cells (Supplemental Figure 2, A and B). PAD2-KO Th2 cells also produced approximately twice more IL-4 and IL-5 than WT counterparts in response to restimulation with anti-CD3 (Figure 2G). There was also a trend of higher IL-13 production by PAD2-KO Th2 cells. Reversely, PAD2-KO Th17 cells had approximately 50% reduction in the level of IL-17A and IL-17F. There was no difference in the production of IFN-γ between WT and PAD2-KO Th1 cells. These results are consistent with our published data showing that overexpression of PAD2 in human PBMC suppressed the expression of Th2 cytokines but increased the level of Th17 cytokines (10). By contrast, deficiency of PAD4 had no reproducible effect on the differentiation of Th cells (Figure 2H). Surprisingly, deficiency of PAD2 only modestly reduced the levels of cit-H3 (Figure 2I). One possible explanation for the modest reduction in the levels of cit-H3 is aberrant expression of other PADs in PAD2-KO Th cells. However, we found no significant change in the transcript level of other PADs in PAD2-KO Th2 cells (Figure 2J).

PAD2 reciprocally regulates the activity of GATA3 and RORγt. GATA3 and RORγt are key transcription factors for Th2 and Th17 cells, respectively. The transcript level of GATA3 was almost two times more in differentiated PAD2-KO Th2 cells than in WT Th2 cells (Figure 3A, left panel). Surprisingly, there was no consistent increase in the protein level of GATA3 (Figure 3B). There was also no reproducible change in the level of nuclear phosphorylated Stat6 (Supplemental Figure 3), the major signaling pathway driving Th2 differentiation. Similarly, the levels of RORγt transcript and protein were comparable between WT and PAD2-KO Th17 cells (Figures 3, A and B). In addition, the transcript levels of other Th17-polarizing transcription factors, including RORα and BATF, were also very comparable between WT and PAD2-KO Th17 cells (Supplemental Figure 4).

We therefore postulated that PAD2 regulated the activity of GATA3 and RORγt. We set up an in vitro luciferase assay in which an IL-13 promoter/reporter, a known GATA3 target, is transactivated by GATA3 in HEK-293T cells, which have no endogenous GATA3 and do not express IL-13. In this system, the transactivation of the IL-13 promoter is solely dependent on exogenous GATA3. Expectedly, ectopic expression of GATA3 was sufficient to induce the activity of the IL-13 promoter approximately 10-fold (Figure 3C). In agreement with our hypothesis, coexpression of PAD2 reduced the GATA3-driven IL-13 promoter activity in a dose-dependent manner (Figure 3C). By contrast, PAD2 dose-dependently enhanced the activity of an IL-17A promoter driven by ectopic RORγt (Figure 3D). Taken together, our data indicate that PAD2 reciprocally regulates the activity of GATA3 and RORγt.

PAD2 physically interacts with GATA3 and RORγt. PAD2 may physically interact with GATA3 and RORγt and citrullinate these 2 transcription factors. We found that anti-GATA3 and anti-RORγt, but not control IgG, coimmunoprecipitated a protein band of approximately 76 kD from Th2 cells and Th17 cells, respectively, but not from PAD2-KO cells (Figure 4, A and B). Reversely, GST-PAD2 was able to pull down full-length GATA3 (Figure 4C) or RORγt (Figure 4D) expressed in HEK-293T cells. We subsequently generated a series of truncation mutants of GATA3 and RORγt and then used GST-PAD2 to pull down the mutants expressed in HEK-293T cells. The N-terminal half but not the zinc finger–containing C-terminal half of GATA3 was sufficient to interact with PAD2 (Figure 4C). The N-terminal half of GATA3 contains 2 transactivation domains. Neither transactivation domain alone was sufficient to interact with PAD2.

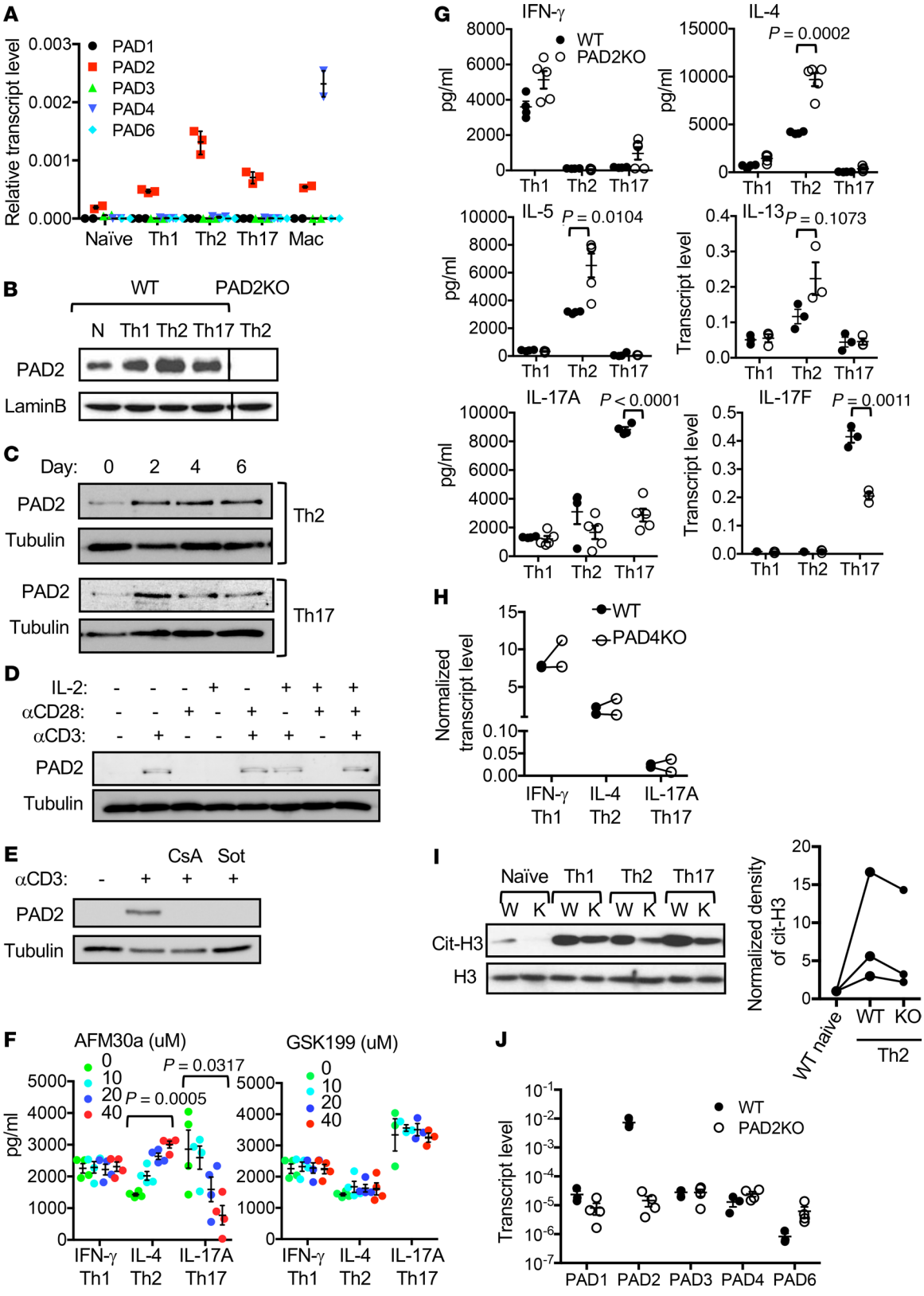

Figure 2. Recapitulating the effects of CI-am by inhibiting PAD2 but not PAD4. (**A**) The transcript levels of indicated PADs in Th cells (n = 3) and macrophages (n = 2) of C57BL/6 mice were measured with real-time PCR and normalized against the levels of actin. (**B**) The levels of PAD2 proteins in indicated C57BL/6 Th cells and PAD2-KO Th2 cells were examined with Western blotting using indicated antibodies. (**C**) At indicated time points during the differentiation of WT Th2 and Th17 cells, the level of PAD2 protein was examined with Western blotting. A parallel gel was probed with anti-tubulin for loading control. (**D** and **E**) WT Th cells were stimulated with anti-CD3, anti-CD28, and/or IL-2 in the absence (**D**) or presence (**E**) of cyclosporine A (CsA) or sotrastaurin (Sot) for 2 days. The level of PAD2 proteins was examined with Western blotting. Representative Western blots from 2 experiments are

shown in **B**–**D**. (**F**) C57BL/6 effector Th cells were generated in the presence of AFM30a (left panel) or GSK199 (right panel) at indicated concentrations. The expression of indicated cytokines by the Th cells after restimulation with anti-CD3 is shown (n = 3–4, 1-way ANOVA)**.** (**G**–**J**) Th cells obtained from WT DBA/1J (**G**–**J**, n = 3–4), PAD2-KO (**G**, **I**, and **J**, n = 3–5), or PAD4-KO (**H**, n = 2) mice were differentiated into Th1, Th2, and Th17 cells for 5 days. The production of indicated cytokines after restimulation with anti-CD3 was measured with ELISA or real-time PCR (**G** and **H**, 2-tailed Student's t test for **G**). Data from the same experiments are connected with lines in **H**. Whole cell extract from WT DBA/1J or PAD2-KO Th cells were examined with Western blotting using anti-citH3 (**I**). A parallel gel was probed with anti-H3 for loading controls. The normalized density of cit-H3 of indicated cells is shown in the dot blot of **I**. The transcript levels of PADs in restimulated WT DBA/1J, and PAD2-KO Th2 cells were quantified with real-time PCR and shown in **J** (n = 3–4).

Instead, a fragment of approximately 120 amino acid residues (61–180 aa) encompassing the intertransactivation domain was pulled down robustly by PAD2. RORγt protein can be divided into a DNA binding domain, a hinge domain, and a ligand binding domain. The ligand binding domain (241–553 aa), but not the other 2 domains, was easily pulled down by GST-PAD2 (Figure 4D). These results suggest that PAD2 interacts with GATA3 and RORγt through their non-DNA binding domains.

Reversely, we used GST-GATA3 and GST-RORγt to pull down various truncated mutants of PAD2. The N-terminal half of PAD2 contains 2 Ig domains (Ig1 and Ig2), whereas its C-terminal half contains the catalytic domain. The full-length PAD2 and its catalytic domain (295–662 aa) were pulled down efficiently by both GST-GATA3 and GST-RORγt (Figure 4E). By contrast, neither Ig domain (1–115 aa or 116–294 aa) was pulled down by GST-GATA3 or GST-RORγt.

GATA3 and RORγt are substrates of PAD2. Our data prompted us to postulate that GATA3 and RORγt are substrates of PAD2. We used biotin-conjugated phenylglyoxal (PG-biotin) to bind citrullinated proteins in extract of Th2 and Th17 cells. PG-biotin–bound citrullinated proteins were then captured with streptavidin and probed with anti-GATA3 or anti-RORγt. This PG pulldown assay is an established method for enriching and identifying citrullinated proteins from heterogeneous protein extract (18–20). We were able to detect cit-GATA3 or cit-RORγt in the nuclear extract, but not the cytoplasmic extract, of stimulated Th2 or Th17 cells, respectively (Figure 5, A–D). However, much less cit-GATA3 and cit-RORγt were detected in WT Th cells differentiated in the presence of Cl-am (Figure 5, A and B) or in PAD2-KO Th cells (Figure 5, C and D). These results indicate that endogenous GATA3 and RORγt are citrullinated by PAD2 in Th2 and Th17 cells, respectively. In parallel, we incubated recombinant GST-GATA3 and GST-RORγt with PAD2 in vitro and then examined the citrullination status of GST-GATA3 and GST-RORγt with Western blotting using F95 (21), a mouse monoclonal IgM raised against a decacitrullinated peptide. As shown in Figure 5, E and F, GST-GATA3 and GST-RORγt, but not GST, became strongly reactive to F95 after in vitro incubation with PAD2.

Citrullination reciprocally modulates the DNA binding ability of GATA3 and RORγt. One possible mechanism by which citrullination regulates the activity of GATA3 and RORγt is altering their DNA binding ability. To test this hypothesis, we carried out electromobility shift assays (EMSA) using recombinant native or PAD2-citrullinated GATA3 and RORγt, shown in Figures 5, E and F. Expectedly, GATA3 bound to a known GATA site from the IL-13 promoter (Figure 5G), whereas RORγt bound to a ROR site from the IL-17A promoter (Figure 5H). In agreement with our hypothesis, PAD2-mediated citrullination attenuated the DNA binding of GATA3 but augmented the DNA binding of RORγt (Figure 5, G and H). By contrast, no DNA binding was detected with native or PAD2-treated GST, and GATA3 or RORγt did not bind to a consensus NF-κB site.

To examine if citrullination also regulated DNA binding of endogenous GATA3 and RORγt, we carried out EMSA by incubating nuclear extract prepared from Th2 or Th17 cells with GATA or ROR probes, respectively. The amount of nuclear extract in each reaction was adjusted to equalize the level of GATA3 or RORγt proteins between WT and PAD2-KO Th cells (Supplemental Figure 5). Expectedly, a fraction of the GATA probes were shifted by extract from Th2 cells (Figure 5I). This shift was blocked by anti-GATA3 but not by control IgG, indicating that the shifted band contained GATA3. Similarly, the ROR probes were shifted by Th17 extract, and the shift was blocked by anti-RORγt (Figure 5J). In agreement with the data shown in Figure 5, G and H, extract from PAD2-KO Th2 cells shifted more GATA probes than its WT counterpart (Figure 5I). Reciprocally, extract from PAD2-KO Th17 cells was less efficient than its WT counterpart in shifting ROR probes (Figure 5J).

Identification of functionally critical citrullination sites of GATA3 and RORγt. To identify the citrullination sites within GATA3 and RORγt, we cut the native and PAD2-citrullinated full-length GST-GATA3 and GST-RORγt shown in Figure 5, E and F, for tandem mass spectrometry (MS/MS). We were able to identify 5 potential citrullination sites in GATA3 (R86, R177, R276, R312, and R330) and 4

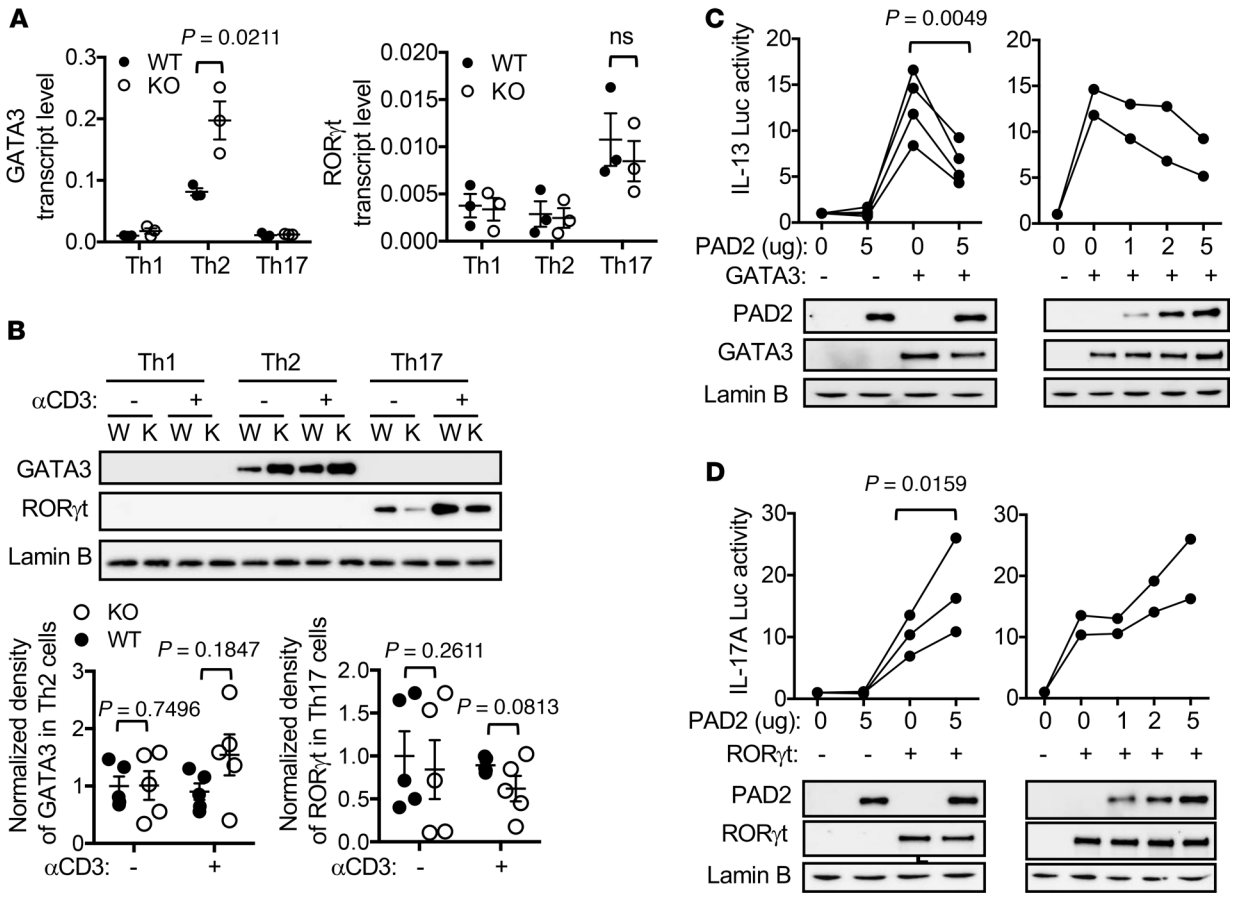

Figure 3. PAD2-mediated citrullination reciprocally regulates the activity of GATA3 and RORγt. (**A** and **B**) Differentiated WT DBA/1J (W) and PAD2-KO (K) Th cells were restimulated with anti-CD3 (**A** and **B**) or left unstimulated (**B**) for 24 hours. The transcript levels of GATA3 and RORγt from 3 independent experiments are shown in **A** (2-tailed Student's *t* test). The levels of GATA3 and RORγt proteins were analyzed with Western blotting. Representative Western blots from 5 independent experiments are shown in **B**. The normalized density of GATA3 and RORγt proteins is shown in the bar graphs of **B** (2-tailed Student's *t* test). The averaged levels in WT cells without restimulation were arbitrarily set as 1. (**C** and **D**) HEK-293 cells were transfected with indicated luciferase reporters and expression vectors. Luciferase activity obtained from cells without exogenous PAD2, GATA3, and RORγt was arbitrarily set as 1 (2-tailed paired Student's *t* test). Data points from the same experiments are connected with lines. Fractions of the cell extract from 2 experiments was subjected to Western blotting using indicated antibodies to demonstrate the expression of exogenous proteins and endogenous Lamin B. Representative Western blots are shown.

potential citrullination sites in RORγt (R56, R59, R77, and R90) (Figure 6, A and B, Supplemental Table 1, and Supplemental Figures 6–14). R276, R312, and R330 of GATA3 are conserved among all GATA members. R276 and R330 are in the corresponding locations of the N-terminal and C-terminal zinc fingers of GATA3 (Figure 6A), respectively. The 4 arginine residues of RORγt are also conserved among RORα and RORβ, as well as several other nuclear hormone receptors, such as RevEr. R56 and R59 of RORγt are located in the C-terminal zinc finger but are distal to P-box, which is responsible for sequence-specific DNA binding, and D-box, which provides a dimerization interface (Figure 6B).

To further determine the impact of each citrullination site on the function of GATA3 and RORγt, we converted each of the arginine residues identified with MS to lysine, which maintains the basic charge but cannot be citrullinated. We found that converting R330 of GATA3 to lysine, but not other R-to-K mutations, markedly reduced the degree of GATA3 citrullination after incubation with PAD2 (Figure 6C). None of the single R-to-K mutations altered the DNA binding of native GATA3 (Supplemental Figure 15A). The DNA binding of the single R-to-K mutants, except the R330K mutant, was still reduced by almost 60% after citrullination by PAD2 (Figure 6D). However, the DNA binding of the R330K mutant was more resistant to PAD2 inhibition (Figure 6D). Interestingly, converting all 5 arginine residues of GATA3 to lysine (5R-K mutant) further increased, albeit marginally, the resistance of GATA3 to PAD2-mediated citrullination and inhibition (Figure 6, C and D). These observations strongly suggest that R330 is the dominant citrullination

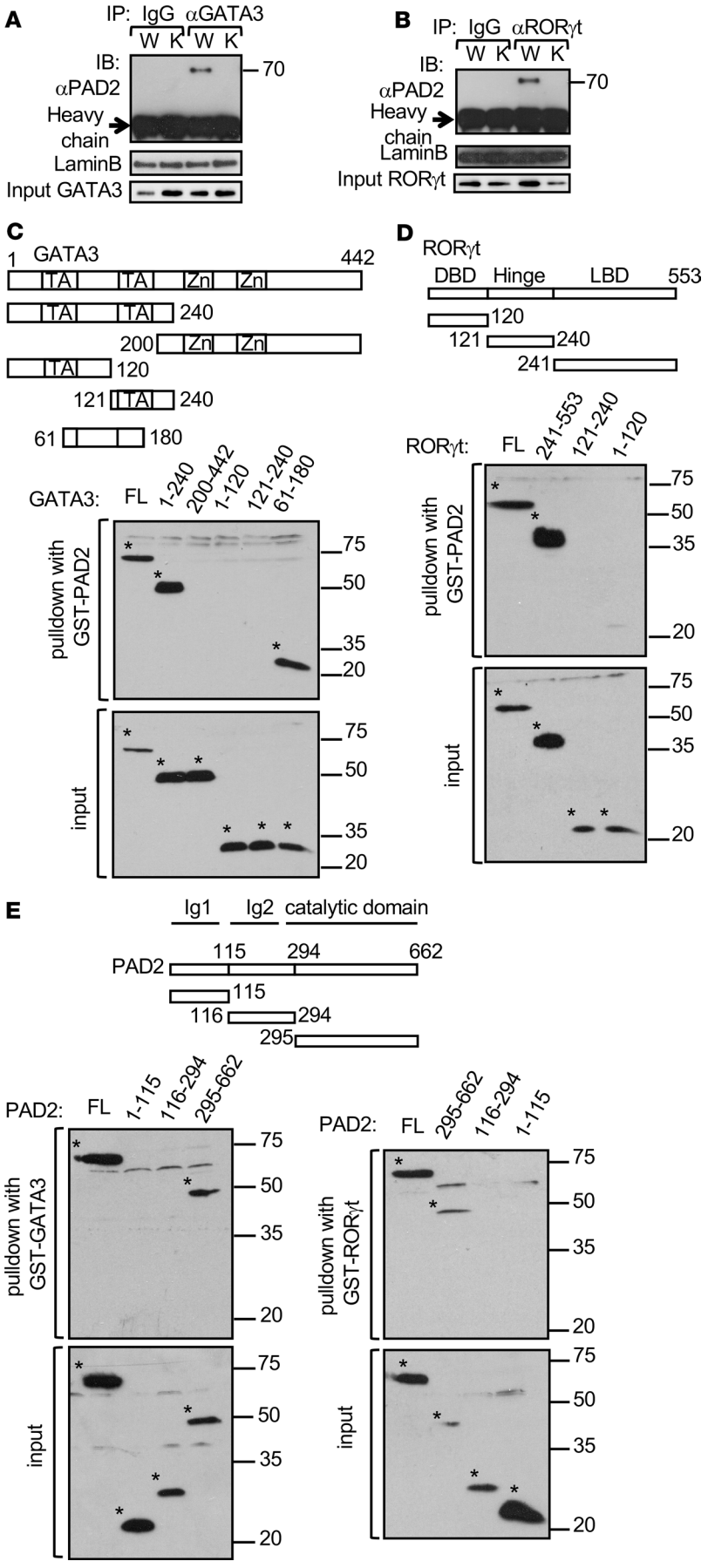

Figure 4. PAD2 physically interacts with GATA3 and RORγt. Whole cells extract was prepared from differentiated WT DBA/1J (W) and PAD2-KO (K) Th2 (**A**) and Th17 (**B**) cells and subjected to immunoprecipitation with anti-GATA3 (**A**), anti-RORγt (**B**) or control IgG (**A** and **B**). The immunoprecipitate was probed with anti-PAD2 in Western blotting (top panels). A fraction of the unprecipitated extract was probed with anti-GATA3 (**A**), anti-RORγt (**B**) and anti-Lamin B as input control (middle and bottom panels). Representative Western blots from 2 experiments are shown. (**C**–**E**) GST-PAD2 (**C** and **D**), GST-GATA3 (**E**, left panels), or GST-RORγt (**E**, right panels) was used to pull down various truncated His-tagged GATA3 (**C**), RORγt (**D**), or PAD2 (**E**) expressed in HEK-293 cells. Whole cell extract from the transfected HEK-293T cells (the bottom panels) and pulldown extract (the top panels) were probed with anti-His. Schematic diagrams of truncated GATA3 (**C**), RORγt (**D**), and PAD2 (**E**) are also shown. The asterisks in the Western blots of **C**–**E** mark exogenous His-GATA3 (**C**), His-RORγt (**D**), and His-PAD2 (**E**). Representative Western blots from 3 experiments are shown in **C**–**E**. TA, transactivation domain; Zn, zinc finger; DBD, DNA binding domain; LBD, ligand binding domain; Ig, immunoglobulin domain; and FL, full length.

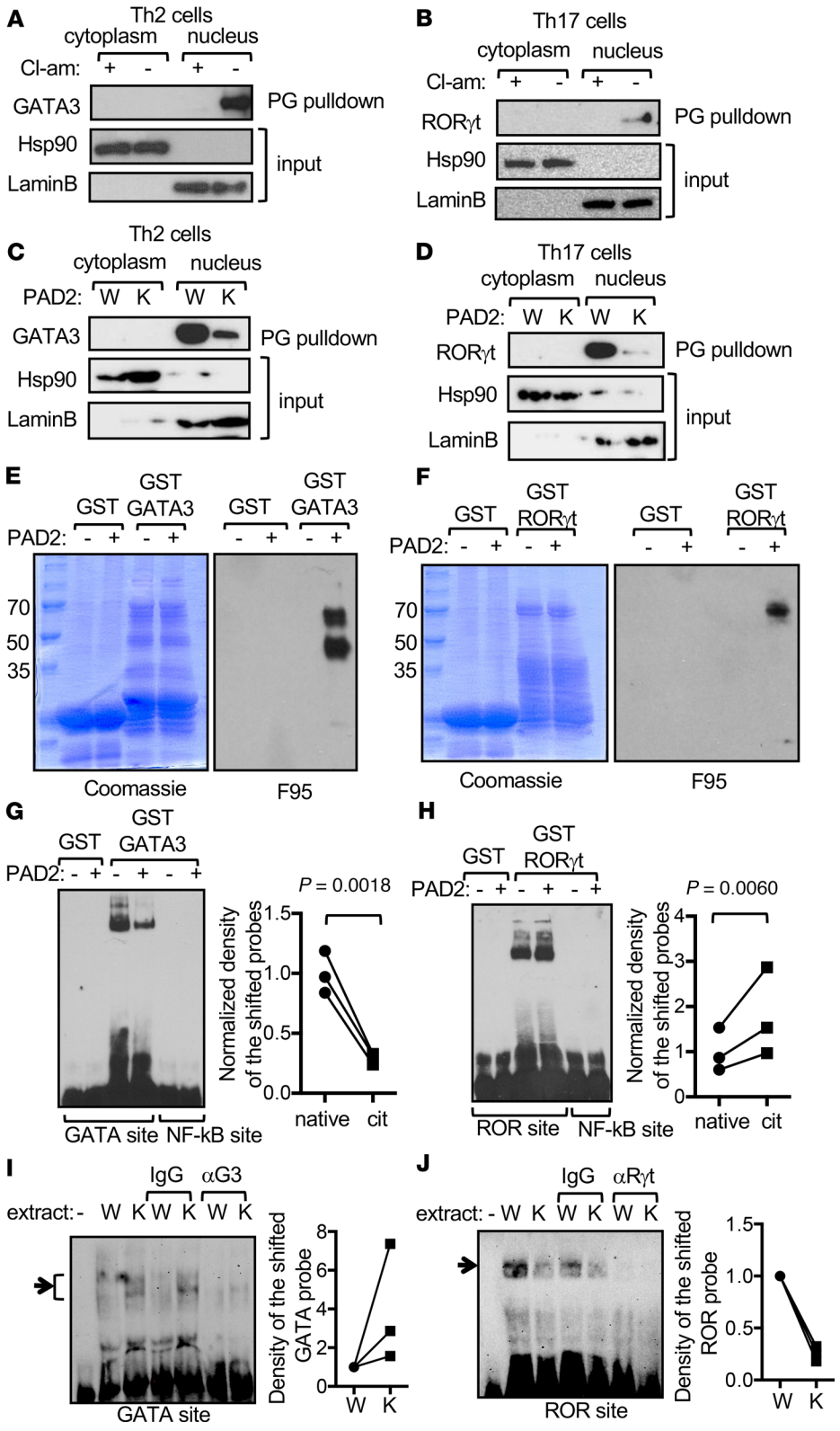

Figure 5. PAD2-mediated citrullination regulates the DNA binding of GATA3 and RORγt. (**A**–**D**) Cytoplasmic and nuclear extract was prepared from WT DBA/1J (**A** and **B**, W in **C** and **D**) or PAD2-KO (K in **C** and **D**) mouse Th2 or Th17 cells differentiated in the presence (+ in **A** and **B**) or absence (**C** and **D**, and – in **A** and **B**) of Cl-am, incubated with PG-biotin, pulled down with streptavidin beads, and probed with anti-GATA3 (**A** and **C**) or anti-RORγt (**B** and **D**) in Western blotting (top panels). A fraction of the PG-biotin–labeled extract prior to pulldown was probed with anti-Hsp90 or anti–Lamin B to serve as input controls (middle and bottom panels). Data shown is from 1 experiment. (**E** and **F**) Recombinant GST, GST-GATA3 (**E**), and GST-RORγt (**F**) were incubated with (+) or without (–) PAD2, fractionated in SDS-PAGE gels, stained with Coomassie blue (left panels), and probed with F95 (right panels) in Western blotting. Data shown are representative blots from at least 2 experiments. (**G** and **H**) The recombinant proteins from **E** and **F** were incubated with indicated DNA probes in EMSA. Representative EMSA gels from 3 experiments are shown. The normalized density of the shifted probes (1 = the averaged density obtained with native proteins) is shown in the dot graphs (2-tailed paired Student's *t* test). Data from the same experiment are connected with lines. (**I** and **J**) EMSA was performed by incubating nuclear extract from WT (W) or PAD2-KO (K) Th2 (**I**) or Th17 (**J**) cells with GATA and ROR probes, respectively, in the absence or presence of IgG, anti-GATA3 (αG3) or anti-RORγt (αRγt). Representative EMSA gels from 3 experiments are shown, and the shifted probes are marked with arrows. The relative density of the shifted probes is shown in the dot graphs. The density from the probes shifted by the WT extract in the absence of IgG was arbitrarily set as 1.

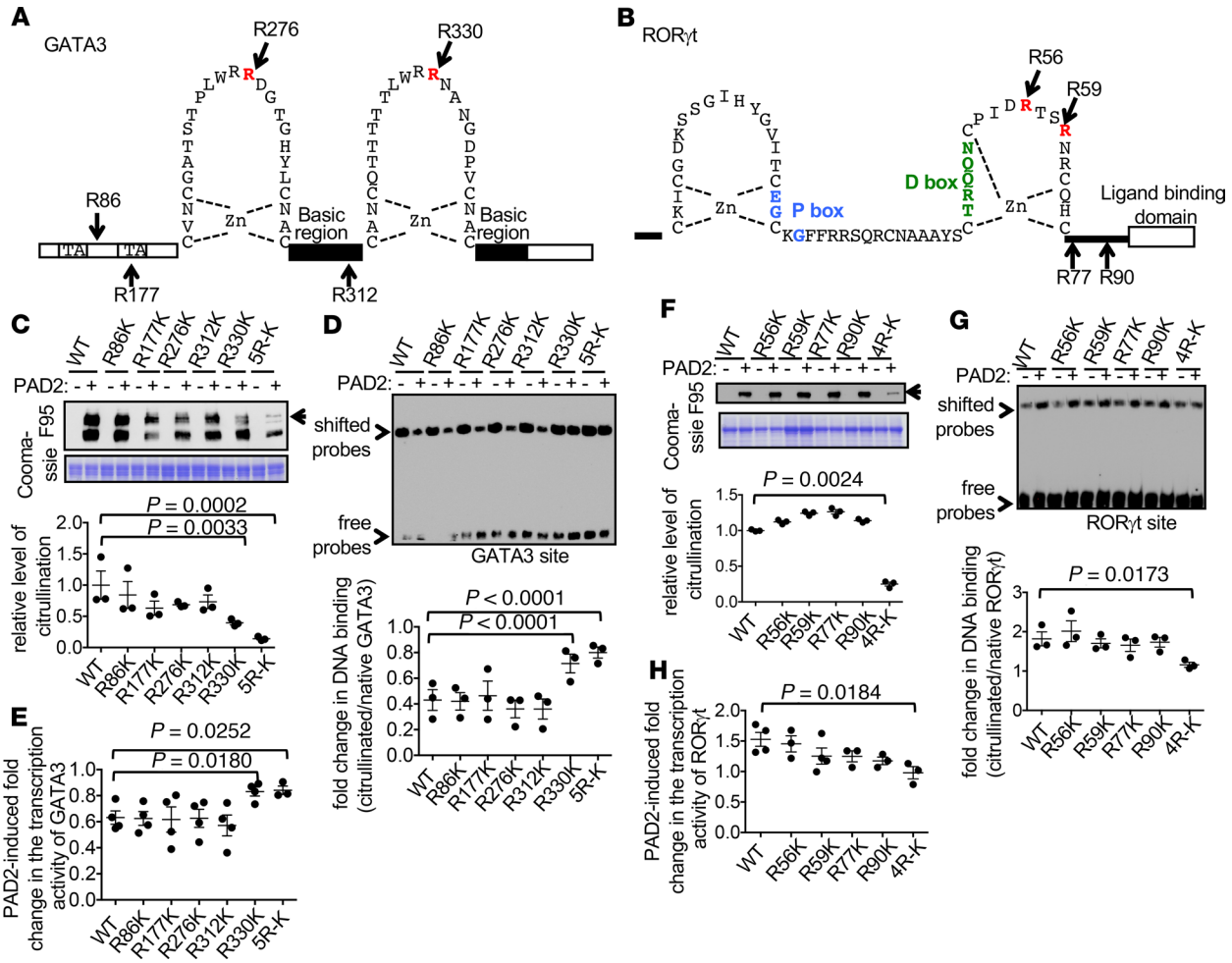

Figure 6. Identification of functionally critical citrullination sites of GATA3 and RORγt. (**A** and **B**) Schematic diagrams of the zinc finger domains of GATA3 (**A**) and RORγt (**B**) are shown. The citrullination sites are marked. TA and Zn represent transactivation domain and zinc ion, respectively. (**C**–**H**) WT and indicated R-to-K mutants of recombinant GATA3 and RORγt were subjected to in vitro citrullination with PAD2 and stained with Coomassie blue as loading controls (bottom panels of **C** and **F**). Their citrullination status was examined with Western blotting using F95 (top panels of **C** and **F**, $n = 3$). The normalized density of the full-length citrullinated proteins (arrows) is shown in the dot plot of **C** and **F**. The native and citrullinated proteins were then incubated with indicated DNA probes in EMSA (**D** and **G**, $n = 3$). The normalized density of the shifted probes is shown in the dot plot of **D** and **G**. The transcription activity of the WT and various R-to-K mutants was examined with luciferase assays in the presence or absence of PAD2 according to the methods described in Figure 3, C and D. The PAD2-induced fold changes in the activity of GATA3 (**E**, $n = 4$) or RORγt (**H**, $n = 4$) are shown. One-way ANOVA with correction for multiple comparison was used in **C**, **D**, **F**, and **G**. Two-tailed Student's *t* test was used to compared WT GATA3 with R330K in **E**, WT GATA3 with 5R-K in **E**, and WT RORγt with 4R-K in **H**.

site and that its citrullination by PAD2 attenuates the DNA binding of GATA3. The alterations in DNA binding of GATA3 were also reflected in its transcriptional activity (Figure 6E). The transactivation of the IL-13 promoter by WT, R86K, R177K, and R312K GATA3 was reduced by almost 40% by PAD2, whereas the transactivation by R330K and 5R-K was more resistant to PAD2 inhibition.

We then used a similar approach to determine the function of each citrullination site of RORγt. None of the single R-to-K mutations altered the DNA binding of native RORγt (Supplemental Figure 15B) or reduced the susceptibility of RORγt to PAD2-mediated citrullination (Figure 6F). In addition, the DNA binding and transcriptional activity of the single R-to-K mutants were still enhanced by PAD2 (Figure 6, G and H). By contrast, converting all 4 arginine residues to lysine rendered RORγt resistant to PAD2-mediated citrullination (Figure 6F, 4R-K). The DNA binding and transcriptional activity of 4R-K also became insensitive to PAD2 (Figure 6, G and H). Thus, the 4 arginine residues comediate the effect of PAD2 on the citrullination, DNA binding, and transcriptional activity of RORγt.

Structural basis of the effects of citrullination on the DNA binding of GATA3 and RORγt. We subsequently modeled the impact of citrullination on the DNA binding of GATA3 and RORγt using the existing

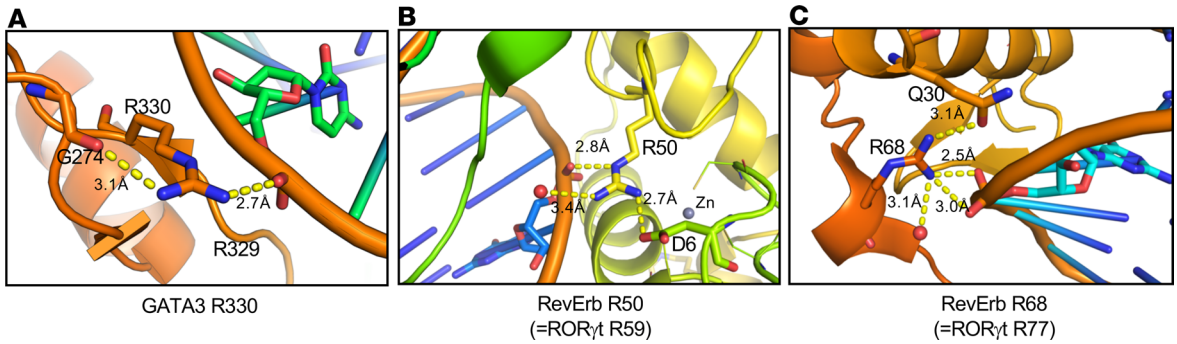

Figure 7. Structural basis of the effects of citrullination on the DNA binding of GATA3 and RORγt. (**A**–**C**) Crystal structures of PDB3VD6 (**A**) and PDB1GA5 (**B** and **C**) were used to generate a hypothesis of the effect of citrullination on the DNA binding of GATA3 and RORγt, respectively. The relevant amino acid residues and their distance between one another were labeled. The gray sphere in **B** represents a zinc ion, whereas the red spheres in **B** and **C** represent water molecules.

crystal structures. Both R329 and R330 are located within the C-terminal zinc finger of GATA3, which is necessary and sufficient for GATA3 to bind to its cognate sequence. While R330 interacts with the sugar phosphate backbone of DNA, R329 makes direct hydrogen bonds and Van der Waals contacts with DNA bases (22). The interaction between R330 and DNA is well resolved and ionically satisfied in the mouse GATA3/DNA structure (Protein Data Bank [PDB] accession number 3VD6). Its side chain binds to DNA phosphate and G274 backbone ketone and very likely holds a β-turn in place. Citrullination of R330 is expected to disrupt its interaction with DNA phosphate and renders R329 to lose contact with DNA (Figure 7A).

There is no published crystal structure of RORγt/DNA. We therefore used the RevErb/DNA crystal structure (PDB1GA5) as the model. Three of the arginine residues of RORγt (R56, R59, and R77) are present in the corresponding positions (R47, R50, and R68) of RevErb, but only R50 and R68 are modeled in the structure. R50 interacts with D6, water, and the DNA sugar phosphate backbone. D6 is involved in a loop holding a Zn ion in place. Disruption of the salt bridge between R50 and D6 by citrullination could make a tighter loop to bind the Zn, therefore yielding a protein with a higher affinity to DNA (Figure 7B). R68 appears to be bonding with Q30, water, and the DNA sugar phosphate backbone. Q30 is part of the C-terminal cap on a helix binding to the major groove of the DNA. Disrupting the R68-Q30 interaction could force the helix structure into the groove for tighter binding (Figure 7C). In addition, Q30 is actually part of another subunit; therefore, R68 could be playing a role in dimerization.

Deficiency of PAD2 increases the susceptibility to allergic airway inflammation. To determine if deficiency of PAD2 can impact Th immune response in vivo, WT and PAD2-KO mice were immunized i.p. with ovalbumin in alum, followed by challenges with aerosolized ovalbumin to induce allergic airway inflammation, a model that is dependent on Th2 cells. Challenges with aerosolized ovalbumin expectedly induced airway inflammation and an increase in the cellularity of bronchial lavage (Figure 8, A and B) in WT mice. In agreement with the effect of PAD2 on in vitro Th2/Th17 differentiation, PAD2-KO immunized/challenged mice were more susceptible to allergic airway inflammation. There were heavier cellular infiltration (Figure 8, A and B), higher percentage and total number of eosinophils ($CD11b^+$/$Siglec\text{-}F^+$) in bronchial lavage (Figure 8, C and D), more mucus-producing cells based on periodic acid-Schiff stain (Figure 8E), and higher levels of IL-4 and IL-13 in their lungs (Figure 8F). Somewhat unexpectedly, substantial levels of Th17 cytokines, including IL-17A and IL-17F, were already present in the lung of unchallenged WT mice, probably because of their DAB/1J genetic background (Figure 8G). The levels of IL-17A and IL-17F were also increased by challenge in WT mice, but the increase was much attenuated or not observed in the lungs of PAD2-KO immunized/challenged mice (Figure 8G). Surprisingly, there was no difference in the transcript level of IL-5 between WT and PAD2-KO mice, despite the difference in the number of eosinophils in lavage, probably due to the overall low level of this cytokine (Supplemental Figure 16).

Discussion

Our data have expanded the physiological role of citrullination to adaptive immune cells. By modulating DNA binding of GATA3 and RORγt, PAD2 can heavily influence the differentiation of Th2 and Th17 cells. This function of PAD2 is seen across species and independent of the genetic background of mouse T cells.

Our data also uncover a mechanism by which PADs regulates gene expression. Citrullination of histones can epigenetically and globally regulating gene expression (23). In addition, citrullination can directly regulate the activity of transcription factors and the transcriptional machinery. For example, citrullination of E2F enhances its acetylation and interaction with BRD4 (24); PAD4 promotes the nuclear translocation of NF-κB p65, and this effect can be partly attributed to the citrullination of this transcription factor, which facilitates its interaction with importin α3 (20, 25); PAD2-mediated citrullination of arginine 1810 of RNA polymerase II (RNAP2) is critical for the interaction between RNAP2 and positive transcription elongation factor b (P-TEFb) (26); here, we show that citrullination of GATA3 and RORγt influences their DNA binding activity.

Our findings are consistent with the published data by Kawalkowska et al. showing that BB–Cl-am (BB-Cl), another pan-PAD inhibitor that is 10-fold more potent than Cl-am, enhanced the serum levels of IL-4 and IL-5 but had no impact on the level of IFN-γ in a collagen-induced arthritis model (27). There was also an increase in the percentage of Th2 cells and a reciprocal decrease in the percentage of Th17 cells, but there was no difference in the percentage of Th1 cells among Th cells in the draining lymph nodes from BB-Cl–treated arthritic mice. However, they also discovered that treating Th cells in vitro with BB-Cl led to apoptosis and reduced the level of all Th cytokines, including IFN-γ, IL-4, and IL-17. We have also found that Th cells, unlike neutrophils, are very sensitive to the cytotoxic effect of BB-Cl; cells were not viable even at 1 μM of BB-Cl. By contrast, Th cells can tolerate Cl-am up to 100 μM concentration.

It was reported that 2-chloroacetamidine (2CA), also a pan-PAD inhibitor, attenuated allergic airway inflammation (28). This in vivo outcome is contradictory to what we observed in PAD2-KO mice and in Cl-am–treated WT mice as well as the results from Kawalkowska's study (27). The cause of this discrepancy is unclear. 2CA also markedly inhibited the proliferation of T cells in vitro. Thus, one possible explanation for the in vivo effect of 2CA is inhibiting the proliferation but not polarization of Th cells. It remains to be determined whether the cytotoxic effect of BB-Cl and the antiproliferative effect of 2CA are due to the suppression of citrullination or off-target effects of these 2 inhibitors. Nevertheless, these observations highlight the potential pitfall of interpreting data generated with PAD inhibitors.

Liu et al. recently reported that both PAD2 and PAD4 were expressed in mouse and human Th cells. They further showed a reduction in the percentage of IL-17A–expressing Th cells in the spleens from imiquimod-treated PAD2-KO FVB mice (29). In addition, Seri et al. demonstrated that PAD4-KO Th cells had no intrinsic defect in differentiating into Th17 cells (30). These findings are consistent with our data. However, similar reduction in the percentage of IL-17A–expressing Th cells was also observed in imiquimod-treated PAD4-KO mice. Imiquimod treatment also reduced the percentage of IFN-γ–producing Th cells in PAD2-KO mice. Furthermore, either AFM30a (at 25 μM) or GSK199 (at 15 μM) inhibited the production of IFN-γ by in vitro differentiated human Th1 cells but reportedly not the production of IL-17A by Th17 cells. The impact on Th2 cells was not described. These latter results are in conflict with ours and those from Kawalkowska's report (27). The cause of the discrepancies is unknown and could be due to differences in the genetic background of animals (FVB vs. DBA/1J and C57BL/6) or mode of in vivo stimulation (TLR7-dependent model vs. Th cell–mediated inflammation).

While deficiency of PAD2 attenuates Th17 differentiation, Raijmakers et al. reported that PAD2-KO mice (in a mixture of 129/SvEv and C57BL/6 genetic background) were still sensitive to experimental autoimmune encephalomyelitis (EAE) (31), a model highly dependent on Th17 cells. Although marked reduction in the level of citrullination was observed in the brain of PAD2-KO mice, it is still possible that other PADs could compensate for the loss of PAD2 in EAE. In addition, deficiency of PAD2 may alter the function of other types of cells, thereby masking impaired Th17 response. Finally, the genetic background of mice may influence the effect of PAD2 on in vivo Th17 response. By contrast, in the TNF transgenic model of RA, in which IL-17 contributes to bone erosions (32), loss of PAD2 reduced arthritis severity and erosions (33).

It was reported that PAD4-mediated NETs are critical for the adjuvant effect of alum (34). While Cl-am is expected to inhibit NETosis, its effect on Th2 polarization very likely overpowers the diminished adjuvant effect of alum, thereby enhancing allergic airway inflammation in our model. Krishnamoorthy et al. recently showed that neutrophil cytoplasts, an end product of NETosis, induce Th17 differentiation and exacerbate airway inflammation caused by house dust mite/LPS (35). Accordingly, PAD4-KO mice developed less airway inflammation. These data are very intriguing in light of our observation that PAD2 deficiency or Cl-am treatment enhanced ovalbumin-induced airway inflammation, which is dependent on

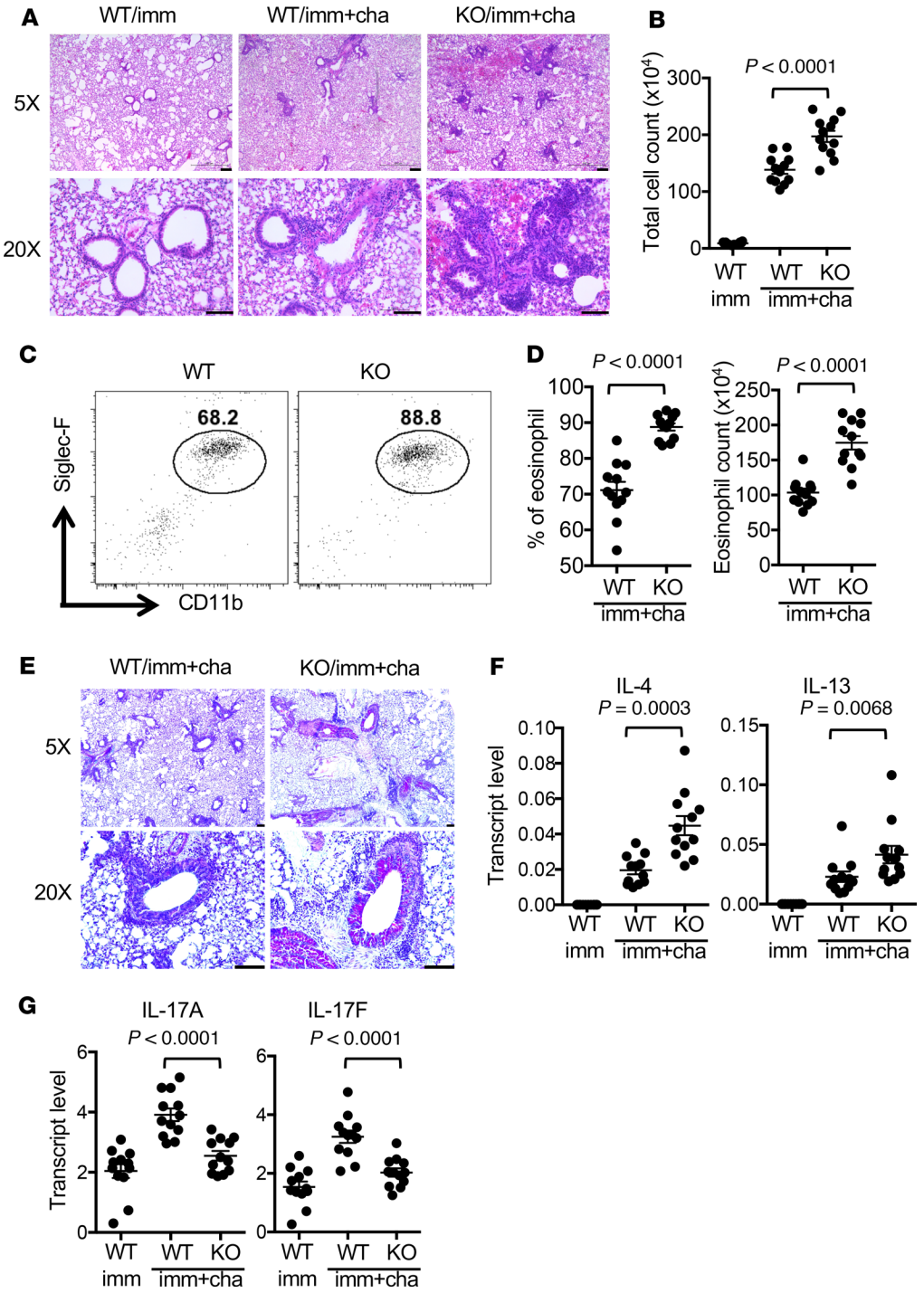

Figure 8. Deficiency of PAD2 increases the susceptibility to allergic airway inflammation. (**A**–**G**) Allergic airway inflammation was induced in WT DBA/1J and PAD2-KO mice (n = 12 per group) according to the protocol described in Methods. Representative H&E staining of lung sections from immunized/unchallenged WT DBA/1J (imm), immunized/challenged WT DBA/1J (WT/imm+cha), and immunized/challenged PAD2-KO (KO/imm+cha) mice were shown in **A**. Scale bars: 100 μm. The total number of cells in bronchial lavage is shown in **B**. Eosinophils in bronchial lavage were identified with FACS as $CD11b^+Siglec\text{-}F^+$ cells. Representative FACS plots are shown in **C**. The percentage and total number of eosinophils in bronchial lavage are shown in **D**. Mucus-producing cells were identified with PAS stain (bright pink stain). Representative sections are shown in **E**. Scale bars: 100 μm. The transcript levels of indicated Th2 and Th17 cytokines in lung tissue were measured with real-time PCR and shown in **F** and **G**, respectively. Statistical analysis was performed with 2-tailed Student's t test.

type 2 immune response. Thus, the impact of PADs on airway inflammation very likely depends on the experimental protocols. It will be interesting to know whether PAD2 and PAD4 influence the clinical outcome of the house dust mite/LPS (HDM/LPS) model and ovalbumin-induced model, respectively.

The locations of the citrullination sites in GATA3 and RORγt are quite intriguing. R276, R312, and R330 of GATA3 are within the DNA binding domain and have been shown to directly participate in the DNA binding (22, 36). Specifically, R330 is buried in the major groove of DNA. By contrast, the 4 arginine residues of RORγt are located outside the DNA binding domain, including the P and D boxes. Thus, the strategic location of the citrullination sites can explain why neutralization of the positive charge of the arginine residues by PADs have opposite effects on the DNA binding of these 2 transcription factors. While R276, R312, and R330 are conserved among all GATA members, the amino acid sequence of the intertransactivation domain, which is required for interaction with PAD2, is quite diverse. Thus, it is still unclear whether PAD2 can regulate the activity of other GATA members. The 4 arginine residues of RORγt are also present in all ROR members and some other nuclear hormone receptors. In addition, the overall structure of the ligand binding domain is conserved among all nuclear hormone receptors (37), raising the possibility that the DNA binding activity of many, if not all, nuclear hormone receptors is susceptible to regulation by PAD2. This scenario may provide an additional explanation for how PAD2 promotes the expression of many estrogen-dependent genes (38).

Our data also underscore the potential benefits and risks of targeting citrullination or PAD2. While inhibiting PAD2 or citrullination in general may be beneficial in Th17 cell–mediated inflammation, such as inflammatory arthritis or colitis, such manipulation may exacerbate Th2 cell–mediated diseases, including allergic airway inflammation. An ideal approach would be to target PADs in a substrate-specific manner. For example, interfering with the interaction between PAD2 and RORγt specifically would attenuate Th17 response without affecting Th2 response. Such manipulations will require in-depth knowledge about the physical interaction between PADs and their individual substrates.

Methods

Human subjects. Peripheral blood of healthy donors was obtained through Brigham and Women's Hospital Specimen Bank.

Mice. The original sources of PAD2-KO and PAD4-KO mice were described previously (4, 31). The mice were backcrossed to DBA/1J mice for 12 generation before use. Littermates were used for all experiments. WT C57BL/6 mice were purchased from the Jackson Laboratory.

Real-time PCR. RNA isolation, reverse transcription, and real-time PCR were performed as previously described (39). Transcript level thus detected was normalized against that of actin or HRPT. The sequences of the primers used are listed in Supplemental Table 2.

Differentiation of mouse primary Th cells. Naive Th cells were stimulated with plate-bound anti-CD3 (catalog 553057, clone 2C11, 1 μg/mL) and soluble anti-CD28 (catalog 553294, clone 37.51, 2 μg/mL) under Th1-skewing (3 ng/mL IL-12 [catalog 210-12P40H] plus 10 μg/mL anti–IL-4 [catalog 559042, clone 11B11]), Th2-skewing (10 ng/mL IL-4 [catalog 214-14] plus 10 μg/mL anti–IFN-γ [catalog 554408, clone XMG1.2]), or Th17-skewing (3 ng/mL TGFβ1 [catalog 240-B-010], 20 ng/mL IL-6 [catalog 406-ML-005] and 10 ng/mL IL-23 [catalog 1887-ML-010/CF]) conditions. Recombinant human IL-2 (catalog Ro-23-6019, 50 U/mL) was added 24 hours later. Cells were harvested after 5 days, washed, and restimulated with plate-bound anti-CD3 (catalog 553057, clone 2C11, 1 μg/mL) overnight. Recombinant human IL-2 (catalog Ro-23-6019) and anti–mouse IL-4 (lot L0412006, clone 11B11) were provided by the National Cancer Institute, Preclinical Repository. IL-4 (catalog 214-14) and IL-12 (catalog 210-12P40H) were purchased from PeproTech. Anti–IFN-γ (catalog 554408, clone XMG1.2), anti-CD3 (catalog 553057, clone 2C11), anti-CD28 (catalog 553294, clone 37.51), and anti-IL-12 (catalog 554475, clone C17.8) were obtained from BD Biosciences. TGFβ1 (catalog 240-B-010), IL-6 (catalog 406-ML-005), and IL-23 (catalog 1887-ML-010/CF) were purchased from R&D Systems. Cl-am (synthesized in house), AFM30 (synthesized in house), and GSK199 (catalog 1549811-53-1, Cayman Chemical) were added at day 0 and maintained during the differentiation of Th cells. The cells were washed thoroughly, resuspended to 1×10^6 cells/mL, and restimulated with anti-CD3 (catalog 553057, clone 2C11, 1 μg/mL) overnight. PMA at 50 ng/mL (catalog P1585, MilliporeSigma), ionomycin at 1 μM (catalog 407950, Calbiochem), cyclosporine A at 20 μM (catalog 12088, Cayman Chemical), and sotrastaurin at 4 μM (catalog 16726, Cayman Chemical) were added wherever indicated.

Cell lines, plasmid, mutagenesis, transfection, and luciferase assay. HEK-293 cells (ATCC, CRL-1573) were maintained in DMEM medium containing 10% heat-inactivated FBS (Hyclone, GE Healthcare Life Science). The full length or truncated cDNA of human PAD2, GATA3, or RORγt was cloned into pCNDA3.1/HisA vector. R-to-K mutants were generated with QuikChange XL Site-Directed Mutagenesis kit (Agilent Technologies) according to manufacturer's instructions. pTK-Renilla luciferase vector and mouse IL-13 promoter-luc (–109; 109 bp upstream to the transcriptional start site of the IL-13 promoter) were described previously (40). Human IL-17A promoter-luc (pGL3E-hIL-17prom[–232]-luc) was obtained from Addgene (41).

Transfection of HEK-293 cells was performed with Effectene Transfection Reagent (Qiagen). The pTK-Renilla luciferase reporter (1 μg) was included in each transfection. Luciferase activity was detected with the Dual-Luciferase Reporter Assay System (Promega) according to the manufacturer's protocol. Values obtained from firefly luciferase signals were normalized to Renilla luciferase activity.

Western blotting. The following antibodies were used: anti-PAD2 (ab183194), anti-GATA3 (ab106625), and anti–citrullinated histone H3 (ab5103) from Abcam; anti–histone H3 (4620S) from Cell Signaling Technology; anti-tubulin (T5168) from Sigma-Aldrich; anti-RORγt (4310958) from eBioscience; anti-Lamin B (sc-6216) from Santa Cruz Biotechnology Inc.; and F95 antibody (MABN328) from EMD Serono. Densitometry readings of Western blots were obtained with ImageJ software (NIH). Loading controls were performed on the same gels after stripping, unless indicated otherwise in the figure legends.

Immunoprecipitation. Th cells were prepared in a lysis buffer containing 20 mM Tris (pH 8.0), 138 mM NaCl, 10% glycerol, 1% Nonidet P-40, 10 mM NaF, 2 mM $NaVO_4$, 1 mM pyrophosphoric acid, and cOmplete protease inhibitors (Roche Applied Science), and centrifuged at 10,967 *g* at 4°C for 15 minutes. The supernatant was incubated with indicated antibodies (2 μg/sample) overnight at 4°C and then incubated with Protein A/G plus-agarose (Santa Cruz Biotechnology Inc.) for 4 hours at 4°C.

GST pulldown assay. The cDNA of human PAD2, human GATA3, or mouse RORγt was cloned into pGEX-4T3 (GE Healthcare), expressed in bacteria (BL21, EMD Millipore) as GST-fused proteins, and prebound to glutathione–agarose beads (MilliporeSigma). The full-length and truncation mutants of PAD2, GATA3, or RORγt were expressed in HEK-293T cells. Whole cell lysate was prepared 48 hours after transfection in the lysis buffer described above. The lysate was incubated with GST-PAD2, GST-GATA3, or GST-RORγt bound beads overnight at 4°C. The captured proteins were then eluted and subjected to Western blotting.

EMSA. EMSAs were performed using the LightShift Chemiluminescent EMSA Kit (Thermo Fisher Scientific). Double-stranded oligonucleotides were generated from biotinylated single-stranded oligonucleotides corresponding to nucleotide fragments of the human IL-13 or IL-17A promoter, which contain GATA-3 (5′-biotin-AATTCAAGATGAGTAAAGATGTGGTTTTCAGATAATGCCCA-3′ and 5′-TGGGCATTATCTGAAAACCACATCTTTACTCATCTTGAATT-3′) or RORγt (5′-biotin-CTGTGCTGACCTCATTTGAGG-3′ and 5′-CCTCAAATGAGGTCAGCACAG-3′) binding sites, were purchased from Integrated DNA Technologies. Nuclear extract from mouse Th2 and Th17 cells was prepared with the NE-PER Nuclear and Cytoplasmic Extraction Reagents (catalog 78833) from Pierce Biotechnology following the manufacturer's protocol. GST-fused recombinant proteins were dialyzed in dialysis buffer (10 mM Tris [pH 7.5], 50 mM KCl, 200 mM NaCl, 1 mM dithiothreitol, 1 mM phenylmethane sulfonyl fluoride, and 10% glycerol; MilliporeSigma) for 16 hours at 4°C with slow stirring. Protein inhibitor cocktail (MilliporeSigma) was diluted to a final concentration of 2.5×. Binding reactions were incubated at room temperature for 30 minutes.

ELISA. Sandwich ELISA was performed with the following antibodies: anti–mouse IFN-γ (catalog 551221)/biotin anti–mouse IFN-γ (catalog 554550) from BD Pharmingen; anti–mouse IL-4 (catalog 554434)/biotin anti–mouse IL-4 (catalog 554390), anti–mouse IL-5 (catalog 554393)/biotin anti–mouse IL-5 (catalog 554397), anti–mouse IL-13 (catalog 14-7133-81)/biotin anti–mouse IL-13 (catalog 13-7135-81), anti–mouse IL-17A (catalog DY421)/biotin anti–mouse IL-17A (catalog DY421), anti–human IL-4 (catalog 14-7049)/biotin anti–human IL-4 (catalog 13-7048), and anti–human IL-17A (catalog 14-7178)/biotin anti–human IL-17A (catalog 13-7179) from eBioscience. Ovalbumin-specific IgE and IgG1 was quantified with anti–ovalbumin Ig E and anti–ovalbumin IgG1 ELISA kits (Cayman Chemical), respectively.

Detection of in vivo citrullinated GATA3 and RORγt. Nuclear and cytoplasmic extract of Th cells was incubated with phenylglyoxal-biotin (PG-biotin) (0.1 mM) in a buffer containing 50 mM HEPES and 20% trichloroacetic acid at 37°C for 30 minutes. After centrifuge, the pellet was resuspended in PBS containing 0.25% SDS, 0.14% 2-Mercaptoethanol (BMe), 0.4 mM HEPES, 2 mM arginine, and 2 mM

NaCl (MilliporeSigma). Biotin-PG–labeled citrullinated proteins were captured with streptavidin–agarose beads (Thermo Fisher Scientific) over night at 4°C.

In vitro citrullination. GST-GATA3 or GST-RORγt recombinant proteins bound to glutathione-agarose beads were incubated with purified recombinant PAD2 (20 mM) in a buffer containing 100 mM HEPES, 100 mM NaCl, 10 mM CaCl2, 0.1 mM EDTA, and 2 mM DTT (MilliporeSigma) for 4 hours at 37°C.

Identification of citrullination sites by LC-MS/MS. In-gel digestion was performed according to a published protocol (42). Liquid chromatography-MS/MS (LC-MS/MS) analysis was performed on a LTQ-Orbitrap Discovery mass spectrometer (Thermo Fisher Scientific) coupled to an Agilent 1200 series HPLC. Samples were pressure loaded onto a hand-pulled 100 μm fused-silica capillary column with a 5-μm tip packed with 10 cm Aqua C18 reverse phase resin (Phenomenex). Peptides were eluted using a 5-hour gradient of 0%–100% Buffer B in Buffer A (Buffer A: 95% water, 5% acetonitrile, 0.1% formic acid; Buffer B: 20% water, 80% acetonitrile, 0.1% formic acid). The flow rate through the column was set to ~400 nL/min, and the spray voltage was set to 2.5 kV. One full MS scan (Fourier transform mass spectrometry; FTMS) was followed by 8 data-dependent MS2 scans (ion trap mass spectrometry; ITMS) of the 8 most abundant ions. These data were used to generate an inclusion mass list of potentially citrullinated peptides. The samples were then subjected to a second MS analysis, whereby a full scan (FTMS) was followed by 4 data-dependent MS2 scans (FTMS) limited to the aforementioned inclusion mass list.

The MS/MS data were searched using the SEQUEST algorithm using a concatenated target/decoy variant of the human or mouse UniProt database. A static modification of +57.02146 Da on cysteine was specified to account for alkylation by iodoacetamide, and a differential modification of +0.984 Da was specified on arginine to account for citrullination. SEQUEST output files were filtered using DTASelect 2.0.

The MS1 and MS2 spectra for putative citrullinated peptides were then manually analyzed. The presence of peptidylcitrulline was determined by an MS1 isotopic envelope matching a predicted envelope for the citrulline-containing peptide (not arginine) and (a) the existence of a fragment (MS2) ion containing the citrulline residue with the expected +0.984 Da mass shift; (b) the existence of a CID neutral loss of isocyanic acid (–43.0058 Da), which is unique to citrulline residues (43); or (c) fragmentation ions for confounding Asn/Gln residence that do not contain a +0.984 Da mass shift, indicative of deamination (<10 ppm error).

Induction of allergic airway inflammation. Mice 8–10 weeks of age were immunized with i.p. injection of 10 μg ovalbumin (Sigma-Aldrich) adsorbed with 1 mg aluminum hydroxide in PBS (200 μL) on days 0 and 14. From day 21, mice were challenged with aerosolized ovalbumin (1% wt/vol) for 30 min/day for 5 consecutive days. Some mice also received either DMSO or Cl-am (10 mg/kg in 10 μL of DMSO) i.p. daily through the entire course. Mice were sacrificed 24 hours after the final challenge. Their lungs were lavaged with 2 mL of PBS. Eosinophils in lavage fluid were identified by flow cytometry, using antibodies against CD11b (M1/70; eBioscience) and Siglec-F (E50-2440; BD Pharmingen). Lung tissues were fixed in 4% paraformaldehyde, embedded in paraffin, sectioned, and then stained with periodic acid-Schiff (PAS) or H&E. RNA was also isolated from lung tissues for real-time PCR analysis. Splenocytes (4 millions/2 mL) were stimulated with ovalbumin (1 mg/mL) for 72 hours. The level of Th cytokines in supernatant was measured with ELISA.

Statistics. The methods used for statistical analysis are indicated in figure legends. The following statistical tests were used: 1-way ANOVA, 1-tailed paired Student's *t* test, 2-tailed paired Student's *t* test, and 2-tailed Student's *t* test. Adjustment of *P* values was conducted if multiple comparison was performed after 1-way ANOVA. The data shown are mean ± SEM, except Figure 2A, which shows mean and range.

Study approval. Human PBMC were obtained through an Brigham and Women's Hospital IRB–approved protocol. All animal experiments were performed in accordance with the institutional guidelines for animal care at Brigham and Women's Hospital.

Author contributions

HHC, MAS, and ICH conceived the idea of citrullination regulating the differentiation of Th cells and cowrote the paper. HHC contributed to the data shown in Figures 1–5 and Supplemental Figures 1–4. BS contributed to the data shown in Figures 1–6 and 8 and Supplemental Figures 5, 15, and 16 and cowrote the paper. As BS has carried out most of the work after HHC left the project, BS is listed first in the author list, a mutual decision between HHC and BS. AS, EW, and PRT contributed to the data shown in Figures 2, 6, and 7; Supplemental Table 1; and Supplemental Figures 6–14 and cowrote the paper. BT contributed to the data shown in Figures 1, 2, 4–6, and 8 and Supplemental Figure 16, and cowrote the paper. MAS, MB, and CLH contributed to the data shown in Figures 2 and 3 and Supplemental Figure 2.

Acknowledgments

This work is supported by an Innovative Research Grant from Rheumatology Research Foundation (ICH) and NIH AR070171 (ICH), AR070253 (BS and HHC), GM079357 (PT), K08 AR065500 (MAS), T32 HL07899 (CLH), F32 GM128231 (AS), and GM110394 (PT and EW).

Address correspondence to: I-Cheng Ho, 60 Fenwood Road, Boston, Massachusetts 02115, USA. Phone: 617.525.1005; Email: iho@bwh.harvard.edu.

1. Witalison EE, Thompson PR, Hofseth LJ. Protein Arginine Deiminases and Associated Citrullination: Physiological Functions and Diseases Associated with Dysregulation. *Curr Drug Targets*. 2015;16(7):700–710.
2. Esposito G, et al. Peptidylarginine deiminase (PAD) 6 is essential for oocyte cytoskeletal sheet formation and female fertility. *Mol Cell Endocrinol*. 2007;273(1-2):25–31.
3. Zhang X, et al. Peptidylarginine deiminase 1-catalyzed histone citrullination is essential for early embryo development. *Sci Rep*. 2016;6:38727.
4. Li P, Li M, Lindberg MR, Kennett MJ, Xiong N, Wang Y. PAD4 is essential for antibacterial innate immunity mediated by neutrophil extracellular traps. *J Exp Med*. 2010;207(9):1853–1862.
5. Demoruelle MK, Deane K. Antibodies to citrullinated protein antigens (ACPAs): clinical and pathophysiologic significance. *Curr Rheumatol Rep*. 2011;13(5):421–430.
6. Uysal H, et al. Antibodies to citrullinated proteins: molecular interactions and arthritogenicity. *Immunol Rev*. 2010;233(1):9–33.
7. Mikuls TR, et al. Porphyromonas gingivalis and disease-related autoantibodies in individuals at increased risk of rheumatoid arthritis. *Arthritis Rheum*. 2012;64(11):3522–3530.
8. Makrygiannakis D, et al. Smoking increases peptidylarginine deiminase 2 enzyme expression in human lungs and increases citrullination in BAL cells. *Ann Rheum Dis*. 2008;67(10):1488–1492.
9. Chang HH, Dwivedi N, Nicholas AP, Ho IC. The W620 Polymorphism in PTPN22 Disrupts Its Interaction With Peptidylarginine Deiminase Type 4 and Enhances Citrullination and NETosis. Arthritis Rheumatol. 2015;67(9):2323–2334.
10. Chang HH, et al. A molecular signature of preclinical rheumatoid arthritis triggered by dysregulated PTPN22. *JCI Insight*. 2016;1(17):e90045.
11. Vahedi G, et al. Helper T-cell identity and evolution of differential transcriptomes and epigenomes. *Immunol Rev*. 2013;252(1):24–40.
12. Maneechotesuwan K, et al. Regulation of Th2 cytokine genes by p38 MAPK-mediated phosphorylation of GATA-3. *J Immunol*. 2007;178(4):2491–2498.
13. Hosokawa H, et al. Methylation of Gata3 protein at Arg-261 regulates transactivation of the Il5 gene in T helper 2 cells. *J Biol Chem*. 2015;290(21):13095–13103.
14. Lim HW, et al. SIRT1 deacetylates RORγt and enhances Th17 cell generation. *J Exp Med*. 2015;212(6):973.
15. Wu Q, et al. Reciprocal regulation of RORγt acetylation and function by p300 and HDAC1. *Sci Rep*. 2015;5:16355.
16. Muth A, et al. Development of a Selective Inhibitor of Protein Arginine Deiminase 2. *J Med Chem*. 2017;60(7):3198–3211.
17. Lewis HD, et al. Inhibition of PAD4 activity is sufficient to disrupt mouse and human NET formation. *Nat Chem Biol*. 2015;11(3):189–191.
18. Lewallen DM, et al. Chemical Proteomic Platform To Identify Citrullinated Proteins. *ACS Chem Biol*. 2015;10(11):2520–2528.
19. Tilvawala R, et al. The Rheumatoid Arthritis-Associated Citrullinome. *Cell Chem Biol*. 2018;25(6):691–704.e6.
20. Sun B, et al. Citrullination of NF-κB p65 promotes its nuclear localization and TLR-induced expression of IL-1β and TNFα. *Sci Immunol*. 2017;2(12):eaal3062.
21. Nicholas AP, Whitaker JN. Preparation of a monoclonal antibody to citrullinated epitopes: its characterization and some applications to immunohistochemistry in human brain. *Glia*. 2002;37(4):328–336.
22. Bates DL, Chen Y, Kim G, Guo L, Chen L. Crystal structures of multiple GATA zinc fingers bound to DNA reveal new insights into DNA recognition and self-association by GATA. *J Mol Biol*. 2008;381(5):1292–1306.
23. Christophorou MA, et al. Citrullination regulates pluripotency and histone H1 binding to chromatin. *Nature*. 2014;507(7490):104–108.
24. Ghari F, et al. Citrullination-acetylation interplay guides E2F-1 activity during the inflammatory response. *Sci Adv*. 2016;2(2):e1501257.
25. Rabadi M, Kim M, D'Agati V, Lee HT. Peptidyl arginine deiminase-4-deficient mice are protected against kidney and liver injury after renal ischemia and reperfusion. *Am J Physiol Renal Physiol*. 2016;311(2):F437–F449.
26. Sharma P, et al. Arginine Citrullination at the C-Terminal Domain Controls RNA Polymerase II Transcription. *Mol Cell*. 2019;73(1):84–96.e7.
27. Kawalkowska J, et al. Abrogation of collagen-induced arthritis by a peptidyl arginine deiminase inhibitor is associated with modulation of T cell-mediated immune responses. *Sci Rep*. 2016;6:26430.
28. Maezawa Y, et al. 2-Chloroacetamidine, a novel immunomodulator, suppresses antigen-induced mouse airway inflammation. *Allergy*. 2015;70(9):1130–1138.
29. Liu Y, et al. Peptidylarginine deiminases 2 and 4 modulate innate and adaptive immune responses in TLR-7-dependent lupus. *JCI Insight*. 2018;3(23):124729.
30. Seri Y, et al. Peptidylarginine deiminase type 4 deficiency reduced arthritis severity in a glucose-6-phosphate isomerase-induced arthritis model. *Sci Rep*. 2015;5:13041.
31. Raijmakers R, et al. Experimental autoimmune encephalomyelitis induction in peptidylarginine deiminase 2 knockout mice. *J Comp Neurol*. 2006;498(2):217–226.

32. Zwerina K, et al. Anti IL-17A therapy inhibits bone loss in TNF-α-mediated murine arthritis by modulation of the T-cell balance. *Eur J Immunol*. 2012;42(2):413–423.
33. Bawadekar M, et al. Peptidylarginine deiminase 2 is required for tumor necrosis factor alpha-induced citrullination and arthritis, but not neutrophil extracellular trap formation. *J Autoimmun*. 2017;80:39–47.
34. Stephen J, Scales HE, Benson RA, Erben D, Garside P, Brewer JM. Neutrophil swarming and extracellular trap formation play a significant role in Alum adjuvant activity. *NPJ Vaccines*. 2017;2:1.
35. Krishnamoorthy N, et al. Neutrophil cytoplasts induce T_H17 differentiation and skew inflammation toward neutrophilia in severe asthma. *Sci Immunol*. 2018;3(26):eaao4747.
36. Chen Y, et al. DNA binding by GATA transcription factor suggests mechanisms of DNA looping and long-range gene regulation. *Cell Rep*. 2012;2(5):1197–1206.
37. Pawlak M, Lefebvre P, Staels B. General molecular biology and architecture of nuclear receptors. *Curr Top Med Chem*. 2012;12(6):486–504.
38. Zhang X, et al. Peptidylarginine deiminase 2-catalyzed histone H3 arginine 26 citrullination facilitates estrogen receptor α target gene activation. *Proc Natl Acad Sci USA*. 2012;109(33):13331–13336.
39. Chang HH, et al. PTPN22 modulates macrophage polarization and susceptibility to dextran sulfate sodium-induced colitis. *J Immunol*. 2013;191(5):2134–2143.
40. Kishikawa H, Sun J, Choi A, Miaw SC, Ho IC. The cell type-specific expression of the murine IL-13 gene is regulated by GATA-3. *J Immunol*. 2001;167(8):4414–4420.
41. Liu XK, Lin X, Gaffen SL. Crucial role for nuclear factor of activated T cells in T cell receptor-mediated regulation of human interleukin-17. *J Biol Chem*. 2004;279(50):52762–52771.
42. Dix MM, Simon GM, Cravatt BF. Global mapping of the topography and magnitude of proteolytic events in apoptosis. *Cell*. 2008;134(4):679–691.
43. Folkersen L, et al. Integration of known DNA, RNA and protein biomarkers provides prediction of anti-TNF response in rheumatoid arthritis: results from the COMBINE study. *Mol Med*. 2016;22:322–328.